Significance of nonperturbative input to the transverse momentum dependent gluon density for hard processes at the LHC

A. A. Grinyuk,[1] A. V. Lipatov,[1,2] G. I. Lykasov,[1] and N. P. Zotov[2]

[1]*Joint Institute for Nuclear Research, Dubna 141980, Moscow Region, Russia*
[2]*Skobeltsyn Institute of Nuclear Physics, Lomonosov Moscow State University, 119991 Moscow, Russia*

We study the role of the nonperturbative input to the transverse momentum dependent (TMD) gluon density in hard processes at the LHC. We derive the input TMD gluon distribution at a low scale $\mu_0^2 \sim 1$ GeV^2 from a fit of inclusive hadron spectra measured at low transverse momenta in pp collisions at the LHC and demonstrate that the best description of these spectra for larger hadron transverse momenta can be achieved by matching the derived TMD gluon distribution with the exact solution of the Balitsky-Fadin-Kuraev-Lipatov equation obtained at low x and small gluon transverse momenta outside the saturation region. Then, we extend the input TMD gluon density to higher μ^2 numerically using the Catani-Ciafoloni-Fiorani-Marchesini gluon evolution equation. Special attention is paid to phenomenological applications of the obtained TMD gluon density to some LHC processes, which are sensitive to the gluon content of a proton.

I. INTRODUCTION

Numerous experimental studies at the LHC are a challenge to theoretical QCD motivated approaches and models. In recent years an understanding has been obtained that the processes at high energies and large momentum transfer containing multiple hard scales require using so-called unintegrated or transverse momentum dependent (TMD) parton density functions (PDFs), which have been used within the framework of the phenomenological k_T-factorization approach [1,2] for many years. In this approach, the TMD parton densities are among the main components that determine its predictive power (see, for example, reviews [3] for more information). The nonperturbative input determines the behavior of the TMD gluon density and production cross sections at a small gluon transverse momentum $k_T \to 0$ and plays a significant role in the k_T factorization [4–9].

In our previous papers [10,11] we obtained the nonperturbative input from the description of the inclusive spectra of hadrons produced in pp collisions at the LHC energies in the midrapidity region at low transverse momenta $k_T \leq 1.5 - 1.6$ GeV and a starting scale $\mu_0^2 = 1$ GeV^2. The proposed input is similar to the TMD gluon density calculated within the popular color-dipole Golec-Biernat-Wüsthoff (GBW) approach [12] at large k_T and differs from it at low transverse momenta. Then, we extended this gluon density to higher μ^2 using the Catani-Ciafoloni-Fiorani-Marchesini (CCFM) evolution equation [13] and considered deep inelastic ep scattering at HERA. We reasonably well described the experimental data on the proton longitudinal structure function $F_L(x, Q^2)$ and the charm and beauty contribution to the structure function $F_2(x, Q^2)$. So, the connection between the soft LHC processes and small x physics at HERA was established.

In the present paper we continue our studies [10,11] and investigate the role of the nonperturbative input to the TMD gluon density in the description of hard processes at the LHC. We improve the initial TMD gluon distribution proposed earlier to describe LHC data on the inclusive charged hadron spectra at higher transverse momenta $2.5 < p_T < 4.5$ GeV and numerically extend it to the whole kinematical region using the CCFM gluon evolution equation. The CCFM equation is the most suitable tool for our study, since it smoothly interpolates between the small-x Balitsky-Fadin-Kuraev-Lipatov (BFKL) [14] gluon dynamics and the conventional Dokshitzer-Gribov-Lipatov-Altarelli-Parisi (DGLAP) [15] one. We extract additional parameters from a fit to the LHC data on the inclusive b-jet production taken by the CMS and ATLAS Collaborations at high p_T and $\sqrt{s} = 7$ TeV. We supply the obtained TMD gluon density with the corresponding TMD valence and sea quark distributions calculated in the approximation, where the sea quarks occur in the last gluon splitting. Finally, we discuss several phenomenological applications of the proposed TMD parton densities to hard LHC processes that are most sensitive to the quark and gluon content of the proton. We use the k_T-factorization approach, which is a commonly recognized tool to investigate hard high-energy processes. Here we see certain advantages in the fact that, even with the leading-order (LO) matrix elements for a hard partonic subprocess, we can take into account a large piece of higher-order QCD corrections, namely, all NLO + NNLO + $\cdots$ terms containing log $1/x$ enhancement.

II. STARTING NONPERTURBATIVE TMD GLUON DENSITY

As was mentioned above, the TMD gluon density was obtained [10] within the soft QCD model as a function of

the proton longitudinal momentum fraction x and two-dimensional gluon transverse momentum $\mathbf{k}_T$ at a fixed value of the scale $\mu_0^2 = 1$ GeV^2. It can be presented in the simple analytical form

$$
\begin{aligned}
f_g^{(0)}(x, \mathbf{k}_T^2, \mu_0^2) = {} & c_0 c_1 (1-x)^b \\
& \times [R_0^2(x)\mathbf{k}_T^2 + c_2(R_0^2(x)\mathbf{k}_T^2)^{a/2}] \\
& \times \exp(-R_0(x)|\mathbf{k}_T| - d[R_0^2(x)\mathbf{k}_T^2]^{3/2}),
\end{aligned}
\tag{1}
$$

where $R_0^2(x) = (x/x_0)^\lambda / \mu_0^2$, $c_0 = 3\sigma_0/4\pi^2\alpha_s$, $x_0 = 4.21 \times 10^{-5}$, $\sigma_0 = 29.12$ mb, $\lambda = 0.22$, and $\alpha_s = 0.2$. The parameters $c_1 = 0.3295$, $c_2 = 2.3$, $a = 0.7$, $b = 12$, and $d = 0.2$ were deduced from the best fit of the LHC data on the inclusive spectra of charged hadrons produced in pp collisions in the midrapidity region at low $p_T \leq 1.6$ GeV. The proposed gluon density differs from the one obtained in the GBW model [12] at $|\mathbf{k}_T| < 1$ GeV and coincides with the GBW gluon at $|\mathbf{k}_T| > 1.5$ GeV. Then, it was treated as a starting distribution for the CCFM evolution equation and successfully applied to the description of the HERA data on the proton structure functions $F_L(x, Q^2)$, $F_2^c(x, Q^2)$, and $F_2^b(x, Q^2)$ [11].

However, the proposed nonperturbative gluon density (1) is not able to describe the LHC data on the inclusive spectrum of charged hadrons at higher transverse momenta $2.5 < p_T < 4.5$ GeV even if additional perturbative QCD (pQCD) corrections [16,17] are taken into account at $p_T > 2$ GeV. Moreover, gluon density (1) decreases much faster when $\mathbf{k}_T^2$ grows compared to the solution of the BFKL equation outside of the saturation region [14,15,18]. Therefore, we modify the gluon density given by (1) at $|\mathbf{k}_T| > 2$–3 GeV to describe the LHC data on the charged hadron production at $2.5 < p_T < 4.5$ GeV. Then we match it with the TMD gluon obtained in Ref. [18] as the solution of the linear BFKL equation at low x, which results in flatter $\mathbf{k}_T^2$ behavior. The modified starting TMD gluon density can be presented in the following form:

$$
\begin{aligned}
f_g^{(0)}(x, \mathbf{k}_T^2, \mu_0^2) = {} & c_0 c_1 (1-x)^b \\
& \times [R_0^2(x)\mathbf{k}_T^2 + c_2(R_0^2(x)\mathbf{k}_T^2)^{a/2}] \\
& \times \exp(-R_0^2(x)\mathbf{k}_T^2 - d[R_0^2(x)\mathbf{k}_T^2]^{3/2}) \\
& + c_0 \left(\frac{x}{x_0}\right)^n \exp\left[-k_0^2 \frac{R_0(x)}{|\mathbf{k}_T|}\right] f_g(x, \mathbf{k}_T^2),
\end{aligned}
\tag{2}
$$

where $k_0 = 1$ GeV, $\mu_0^2 = 1.1$ GeV^2, and $n \simeq 0.81$. The function $f_g(x, \mathbf{k}_T^2)$ obeying the BFKL equation at not very large $\mathbf{k}_T^2$ reads [18]

$$
f_g(x, \mathbf{k}_T^2) = \alpha_s^2 x^{-\Delta} t^{-1/2} \frac{1}{v} \exp\left[-\frac{\pi \ln^2 v}{t}\right],
\tag{3}
$$

where $t = 14\alpha_s N_c \zeta(3) \ln(1/x)$, $v = |\mathbf{k}_T|/\Lambda_{\text{QCD}}$, and $\Delta = 4\alpha_s N_c \ln 2/\pi$. It is important that the third term in (2) is only nonzero at $|\mathbf{k}_T| \ll \Lambda_{\text{QCD}}(1/x)^\delta$ with $\delta = \alpha_s N_c$. The details of the calculation and the relation between the TMD gluon density and the inclusive hadron spectra $\rho_h(y \simeq 0, p_T) \equiv E d^3\sigma/d^3 p$ are given in our previous papers [10,11]. These spectra are presented as a sum of two parts [16,17]:

$$
\rho_h(y \simeq 0, p_T) = \rho_q(y \simeq 0, p_T) + \rho_g(y \simeq 0, p_T),
\tag{4}
$$

where ρ_q is the quark contribution calculated within the quark-gluon string model [19–21] and ρ_g is the gluon contribution, which can be calculated using the proposed TMD gluon density (2) and (3). Taking into account the energy $\sqrt{s}$ dependence of the ρ_q and ρ_g parts, the spectrum $\rho_h(y \simeq 0, p_T)$ can be written in the following form:

$$
\begin{aligned}
& \rho_h(y \simeq 0, p_T) \\
& = \left[\phi_q(y \simeq 0, p_T) + \phi_g(y \simeq 0, p_T)\left(1 - \frac{\sigma_{nd}}{g(s/s_0)^\Delta}\right)\right] \\
& \quad \times g(s/s_0)^\Delta,
\end{aligned}
\tag{5}
$$

where $g = 21$ mb, $\Delta = \alpha_P(0) - 1 \simeq 0.12$, $\alpha_P(0)$ is the Pomeron intercept and σ_{nd} is the nondiffractive cross section given by the sum of n Pomeron chain production cross sections. The functions $\phi_q(y \simeq 0, p_T)$ and $\phi_g(y \simeq 0, p_T)$ are evaluated in [16,17] and can be presented as

$$
\phi_q(y \simeq 0, p_T) = A_q \exp(-p_T/C_q),
\tag{6}
$$

$$
\phi_g(y \simeq 0, p_T) = A_g \sqrt{p_T} \exp(-p_T/C_g),
\tag{7}
$$

where the parameters $A_q = 3.68$ GeV^{-2}, $A_g = 1.7249$ GeV^{-2}, $C_q = 0.147$ GeV, and $C_g = 0.289$ GeV were obtained from the combined fit of the NA61 [22] and LHC [23] data taken at different energies $\sqrt{s}$ [16]. These parameters, of course, differ from the ones obtained earlier [10] due to another form of TMD gluon density (2) and (3) used in the fit procedure. The latter leads, in addition, to the values of the parameters $d = 0$ and $a = 0.3$ in (2). In this way the LHC data [23] are fitted with $\chi^2/n.d.f = 0.998$. The parameters $b = 6.57$ and $\alpha_s = 0.18$ were obtained from the best fit of the CMS data on the inclusive b-jet production at $|y| < 0.5$ (see below). Let us stress here that since the parameters of nonperturbative input (2) and (3) were obtained from the description of the LHC and NA61 data [22,23], possible higher-order corrections (see, for example, [24–26]) to the leading-order
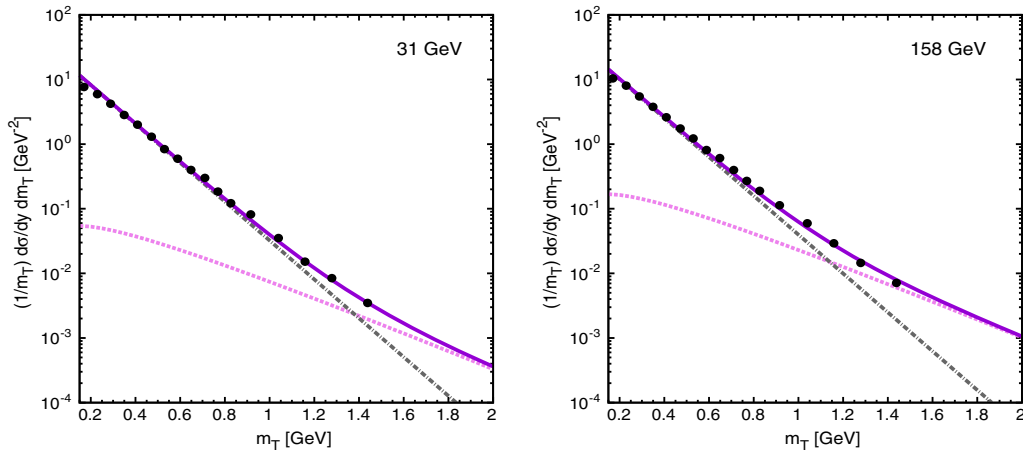
FIG. 1.   The inclusive cross sections of the π^- meson production in the pp collisions at the initial momenta 31 and 158 GeV/c as a function of the transverse mass. The dashed and dash-dotted curves correspond to the gluon and quark contributions, respectively. The solid curves represent their sum. The experimental data are from NA61 [22].

BFKL-motivated $\mathbf{k}_T$ dependence of the proposed gluon input at low x (as well as saturation dynamics) are effectively included.

The inclusive spectra of π^- mesons produced in pp collisions at the initial momenta 31 and 158 GeV/c are presented in Fig. 1 as a function of the transverse mass $m_T = \sqrt{m_\pi^2 + p_T^2}$. Using the first part of the spectrum $\phi_q(y \simeq 0, p_T)$, connected with the quark contribution in the conventional string model [19], one can reasonably describe the NA61 data [22] at low $m_T < 1$ GeV. The inclusion of the second part of the spectrum, which is due to the gluon contribution, allows us to describe the NA61 data up to $m_T \sim 1.5$ GeV. A similar description of the experimental data on the inclusive spectra of charged hadrons (mainly pions and/or kaons) is achieved at the LHC (see Fig. 2). In addition to the soft part, we include the pQCD corrections [16,17]. The latter, made at LO, are divergent at low transverse momenta. Therefore, the kinematical region $p_T \sim 1.8$–2.2 GeV can be treated as the matching region of the nonperturbative QCD (soft QCD) and pQCD calculations. One can see that the inclusive hadron spectra at the LHC can be well described in a wide region of transverse momenta by matching these two approaches, and the proposed input TMD gluon density (2) and (3) plays a crucial role in the description of these data at low hadron transverse momenta.

III. CCFM-EVOLVED TMD PARTON DENSITIES

The average gluon transverse momentum $\langle|\mathbf{k}_T|\rangle$, generated by the TMD gluon distribution defined above, is $\langle|\mathbf{k}_T|\rangle \sim 1.9$ GeV at $10^{-7} < x < 1$, which is close to the nonperturbative QCD regime. Therefore, we can treat the proposed TMD gluon density as a starting one and apply the CCFM equation to extend it to the whole kinematical region. The CCFM evolution equation resums large logarithms $\alpha_s^n \ln^n 1/(1-x)$ in addition to $\alpha_s^n \ln^n 1/x$ ones and

introduces angular ordering of initial emissions to correctly treat gluon coherence effects. In the limit of asymptotic energies, it is almost equivalent to BFKL, but also similar to the DGLAP evolution for large x and high μ^2 [13].

In the leading logarithmic approximation, the CCFM equation with respect to the evolution (factorization) scale μ^2 can be written as [13]

$$f_g(x, \mathbf{k}_T^2, \mu^2) = f_g^{(0)}(x, \mathbf{k}_T^2, \mu_0^2)\Delta_s(\mu^2, \mu_0^2)$$
$$+ \int \frac{dz}{z} \int \frac{dq^2}{q^2} \theta(\mu - zq)\Delta_s(\mu^2, z^2 q^2)P_{gg}$$
$$\times (z, q^2, \mathbf{k}_T^2)f_g(x/z, \mathbf{k}_T'^2, q^2), \qquad (8)$$

where $\mathbf{k}'_T = \mathbf{q}(1-z) + \mathbf{k}_T$ and the Sudakov form factor $\Delta_s(q_1^2, q_2^2)$ describes the probability of no radiation between q_2^2 and q_1^2. The first term in the CCFM equation (8), which is the initial TMD gluon density multiplied by the Sudakov form factor $\Delta_s(\mu^2, \mu_0^2)$, makes the contribution of nonresolvable branchings between the starting scale μ_0^2 and the factorization scale μ^2, the second term describes the details of the QCD evolution expressed by the convolution of the CCFM splitting function $P_{gg}(z, q^2, \mathbf{k}_T^2)$ with the gluon density $f_g(x, \mathbf{k}_T^2, \mu^2)$ and the Sudakov form factor $\Delta_s(\mu^2, q^2)$, and the theta function introduces the angular ordering condition. The evolution scale μ^2 is defined by the maximum allowed angle for any gluon emission [13].

The CCFM equation (8) describes only the emission of gluons, while quark emissions are left aside. In order to calculate the TMD valence quark densities, we have to replace in (8) the gluon splitting function $P_{gg}(z, q^2, \mathbf{k}_T^2)$ by the quark one $P_{qq}(z, q^2, \mathbf{k}_T^2)$ [27,28]. The starting TMD valence quark distribution can be parameterized using standard collinear PDFs $xq_v(x, \mu^2)$ as
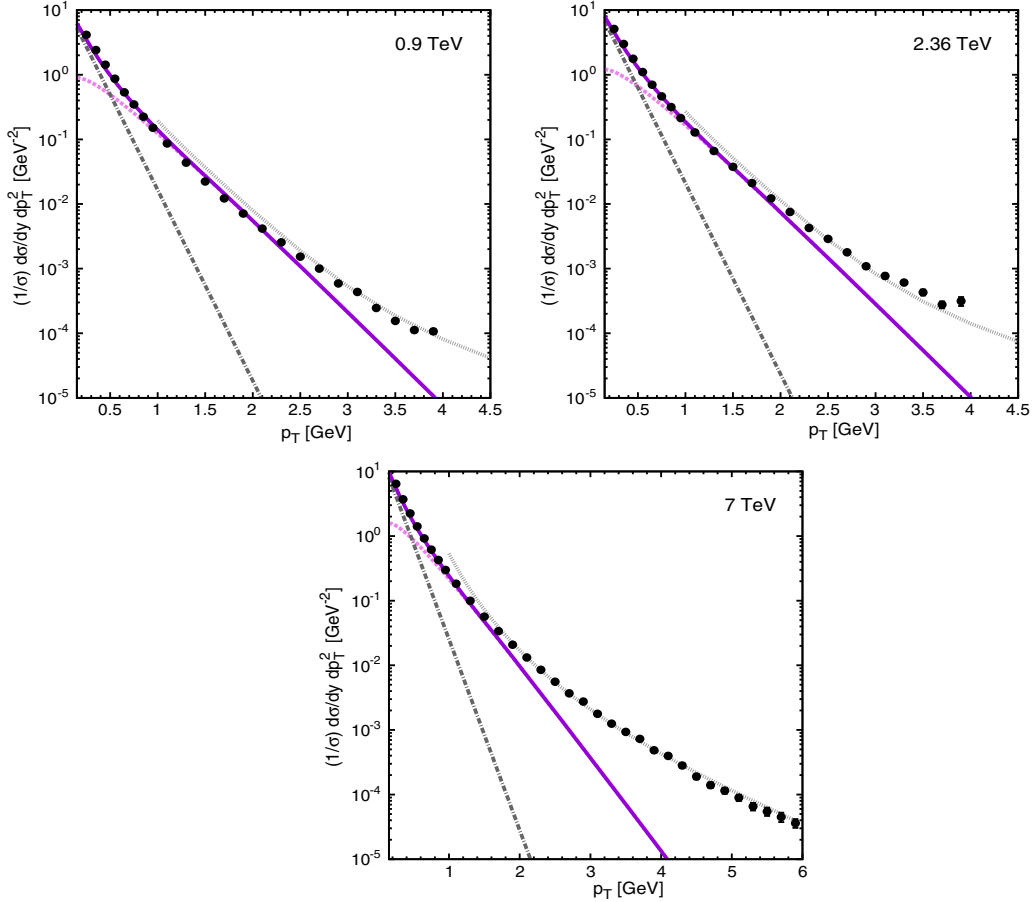
FIG. 2. The inclusive cross sections of the hadron production in the pp collisions at the LHC as a function of the transverse momentum. The dashed and dash-dotted curves correspond to the gluon and quark contributions, respectively. The solid curves represent their sum. The dotted curves correspond to the sum of the soft QCD and pQCD predictions as described in the text. The experimental data are from ATLAS and CMS [23].

$$f_{q_v}^{(0)}(x, \mathbf{k}_T^2, \mu_0^2) = xq_v(x, \mu_0^2) \frac{2}{\mu_0^2} \exp\left[-\frac{\mathbf{k}_T^2}{\mu_0^2/2}\right]. \quad (9)$$

Numerically, we applied the LO parton densities from the Martin-Stirling-Thorne-Watt 2008 set [29]. The exact analytical expressions for the splitting functions $P_{gg}(z, q^2, \mathbf{k}_T^2)$ and $P_{qq}(z, q^2, \mathbf{k}_T^2)$ and the Sudakov form factor can be found, for example, in Ref. [30]. Concerning the TMD sea quark density, we calculate it using the approximation where the sea quarks occur in the last gluon-to-quark splitting. At the next-to-leading logarithmic accuracy $\alpha_s(\alpha_s \ln x)^n$, the TMD sea quark distribution can be written [7] as

$$f_{q_s}(x, \mathbf{k}_T^2, \mu^2) = \int_x^1 \frac{dz}{z} \int d\mathbf{q}_T^2 \frac{1}{\mathbf{\Delta}^2} \frac{\alpha_s}{2\pi} P_{qg}$$
$$\times (z, \mathbf{q}_T^2, \mathbf{\Delta}^2) f_g(x/z, \mathbf{q}_T^2, \bar{\mu}^2), \quad (10)$$

where z is the fraction of the gluon light cone momentum carried out by the quark and $\mathbf{\Delta} = \mathbf{k}_T - z\mathbf{q}_T$. The sea quark

evolution is driven by the off-shell gluon-to-quark splitting function $P_{qg}(z, \mathbf{q}_T^2, \mathbf{\Delta}^2)$ [31]:

$$P_{qg}(z, \mathbf{q}_T^2, \mathbf{\Delta}^2) = T_R \left(\frac{\mathbf{\Delta}^2}{\mathbf{\Delta}^2 + z(1-z)\mathbf{q}_T^2}\right)^2$$
$$\times \left[(1-z)^2 + z^2 + 4z^2(1-z)^2 \frac{\mathbf{q}_T^2}{\mathbf{\Delta}^2}\right], \quad (11)$$

where $T_R = 1/2$. The splitting function $P_{qg}(z, \mathbf{q}_T^2, \mathbf{\Delta}^2)$ was obtained by generalizing to finite transverse momenta of the two-particle irreducible kernel expansion [32]. It takes into account the small-x enhanced transverse momentum dependence up to all orders in the strong coupling constant and reduces to the conventional splitting function at the lowest order for $|\mathbf{q}_T| \to 0$. The scale $\bar{\mu}^2$ was defined [33] from the angular ordering condition which is natural from the point of view of the CCFM evolution: $\bar{\mu}^2 = \mathbf{\Delta}^2/(1-z)^2 + \mathbf{q}_T^2/(1-z)$.
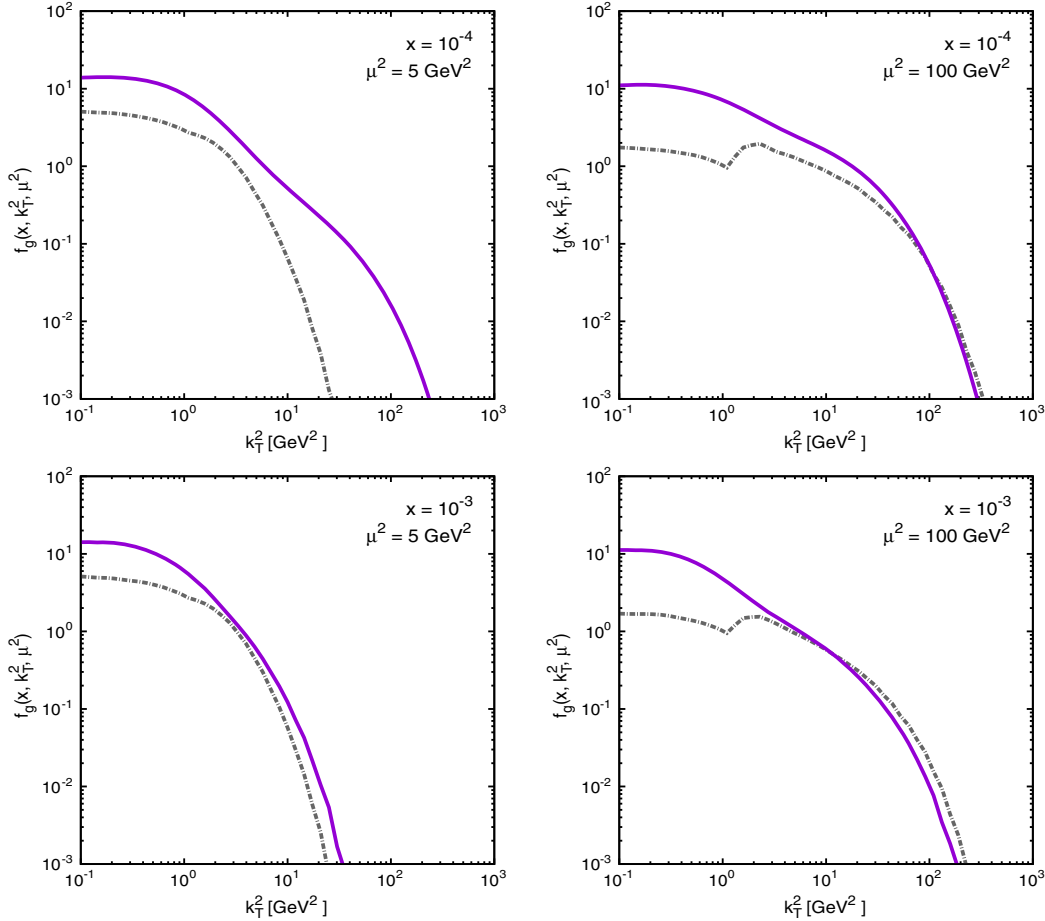
FIG. 3. The CCFM-evolved TMD gluon densities in the proton calculated as a function of the gluon transverse momentum squared $\mathbf{k}_T^2$ at different x and μ^2. The solid and dashed curves correspond to the proposed MD2015 and A0 gluon densities, respectively.

The CCFM evolution equation with the starting TMD gluon and quark distributions given by (2), (3), and (9) was solved numerically[1] in the leading logarithmic approximation using the UPDFEVOLV routine [30]. Thus, the TMD gluon and valence quark densities were obtained for any x, $\mathbf{k}_T^2$, and μ^2 values. The TMD sea quark distributions can be evaluated according to (10) and (11).

The gluon density $f_g(x, \mathbf{k}_T^2, \mu^2)$ obtained according to (2), (3), and (8), labeled below as *Moscow-Dubna 2015* (MD2015), is shown in Fig. 3 as a function of $\mathbf{k}_T^2$ for different values of x and μ^2. Additionally, we plot the TMD gluon distribution [34] (namely, the set A0) which is widely discussed in the literature and commonly used in the applications. One can observe some difference in the absolute normalization and shape between both TMD gluon distributions. Below, we will consider the corresponding phenomenological consequences for several LHC processes.

IV. PHENOMENOLOGICAL APPLICATIONS

We are now in a position to apply the proposed TMD parton densities to some processes studied at hadron colliders. In the present paper we consider the inclusive production of b jets and B^+ and D^* mesons as well as the associated production of $W^\pm$ or Z/γ^* bosons and hadronic jets at the LHC conditions. We also study the charm and beauty contribution to the proton structure function $F_2(x, Q^2)$ and the longitudinal proton structure function $F_L(x, Q^2)$. These processes are known to be strongly sensitive to the gluon and/or quark content of the proton.

According to the k_T-factorization prescription [1,2], the cross sections of the processes under consideration can be written as

$$\sigma = \int dx_1 dx_2 \int d\mathbf{k}_{1T}^2 d\mathbf{k}_{2T}^2 f_{q/g}(x_1, \mathbf{k}_{1T}^2, \mu^2)$$
$$\times f_{q/g}(x_2, \mathbf{k}_{2T}^2, \mu^2) \times d\hat{\sigma}(x_1, x_2, \mathbf{k}_{1T}^2, \mathbf{k}_{2T}^2, \mu^2), \quad (12)$$

where $\hat{\sigma}(x_1, x_2, \mathbf{k}_{1T}^2, \mathbf{k}_{2T}^2, \mu^2)$ are relevant off-shell (depending on the transverse momenta of incoming particles)
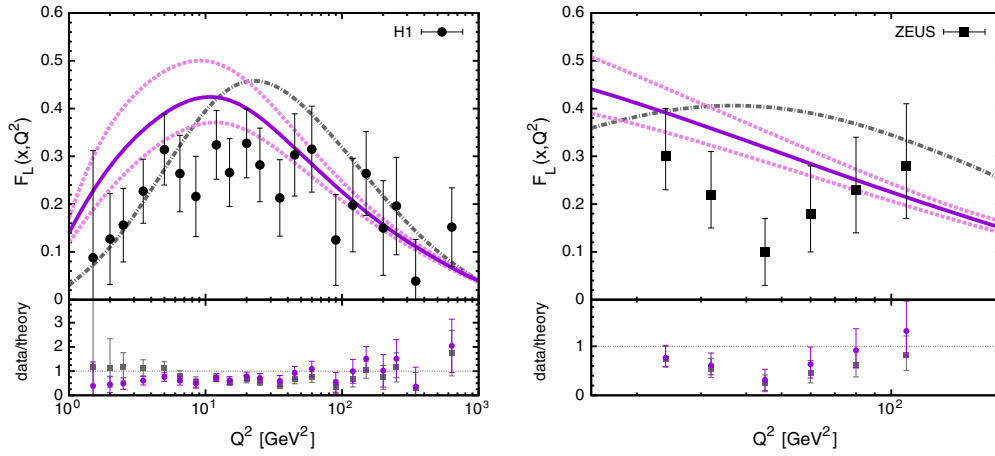
---

[1]The authors are very grateful to Hannes Jung for providing us with the appropriate numerical code.

FIG. 4.   The longitudinal proton structure function $F_L(x, Q^2)$ as a function of Q^2. The solid curve corresponds to the predictions obtained with the proposed MD2015 gluon density. The upper and lower dashed curves correspond to the usual scale variations in these calculations. The dash-dotted curve represents the results obtained with the A0 gluon. The experimental data are from H1 [41] and ZEUS [42]. In the ZEUS measurements the ratio Q^2/x is a constant for each bin, which corresponds to $y = 0.71$ and $\sqrt{s} = 225$ GeV, where $y = Q^2/xs$.

partonic cross sections. The detailed description of the calculation steps (including the evaluation of the off-shell amplitudes) can be found in our previous papers [35–38]. Here we specify only the essential numerical parameters. Following Ref. [39], we set the charmed and beauty quark masses $m_c = 1.4$ GeV and $m_b = 4.75$ GeV, D^* and B^+ meson masses $m_{D^*} = 2.01$ GeV and $m_{B^+} = 5.28$ GeV, the masses of gauge bosons $m_W = 80.403$ GeV and $m_Z = 91.1876$ GeV, Z boson decay width $\Gamma_Z = 2.4952$ GeV, and the Weinberg mixing angle $\sin^2 \theta_W = 0.231$. We use the two-loop formula for the strong coupling constant (as it is implemented in the UPDFEVOLV routine) with $n_f = 4$ active quark flavors at $\Lambda_{QCD} = 200$ MeV and apply the running QCD and QED coupling constants. We use the factorization and renormalization scales μ_F and μ_R according to the process under consideration [35–38]. Additionally, we estimate the theoretical uncertainty coming from the renormalization scale.

Multidimensional integration was performed by the Monte Carlo technique, using the routine VEGAS [40]. The corresponding C++ code is available from the authors on request.

A. Proton structure functions F_2^c, F_2^b, and F_L

The charm and beauty contributions to the proton structure function $F_2(x, Q^2)$ and the longitudinal structure function $F_L(x, Q^2)$ are directly connected to the gluon content of the proton. The structure function $F_L(x, Q^2)$ is equal to zero in the parton model with spin $1/2$ partons and only has nonzero values within the pQCD. The experimental data on these structure functions were obtained [41–45] by the H1 and ZEUS Collaborations at HERA. Our consideration is based on the formalism [35], and here we present the main results only.

The results of our calculations are presented in Figs. 4–6. The solid curves correspond to the predictions obtained with the MD2015 gluon distribution, the upper and lower dashed curves represent the estimate of the corresponding theoretical uncertainties (as given by the usual scale variations), and the dash-dotted curves correspond to the results obtained with the A0 gluon density. Additionally, we plot the data and theory ratios for the longitudinal structure function $F_L(x, Q^2)$. One can see that the predictions corresponding to the proposed MD2015 gluon distribution agree well with the H1 and ZEUS data in the whole kinematical region of x and Q^2 within the theoretical and experimental uncertainties. It only tends to slightly overestimate the F_L data [41] at very low Q^2 but still agrees with them within the theoretical and experimental uncertainties. Therefore, the main conclusion of Refs. [10,11], where the link between soft processes at the LHC and low-x physics at HERA was pointed out, is confirmed. At the same time, the A0 gluon density does not reproduce the shape of the structure functions F_2^c and F_2^b at low Q^2. It means that the influence of the shape and other parameters of the initial nonperturbative gluon distribution on the description of the experimental data is significant for a wide region of x and Q^2. We conclude that the best description of the HERA data [41–45] is achieved with the MD2015 gluon density.

B. Inclusive b-jet production

As is well known, beauty quarks at the LHC energies are produced mainly via a standard QCD gluon-gluon fusion subprocess; therefore, the corresponding total and differential cross sections are strongly sensitive to the gluon content of the proton. In the k_T-factorization approach this was demonstrated in our previous paper [36]. Below, we probe the MD2015 gluon density in the inclusive b-jet
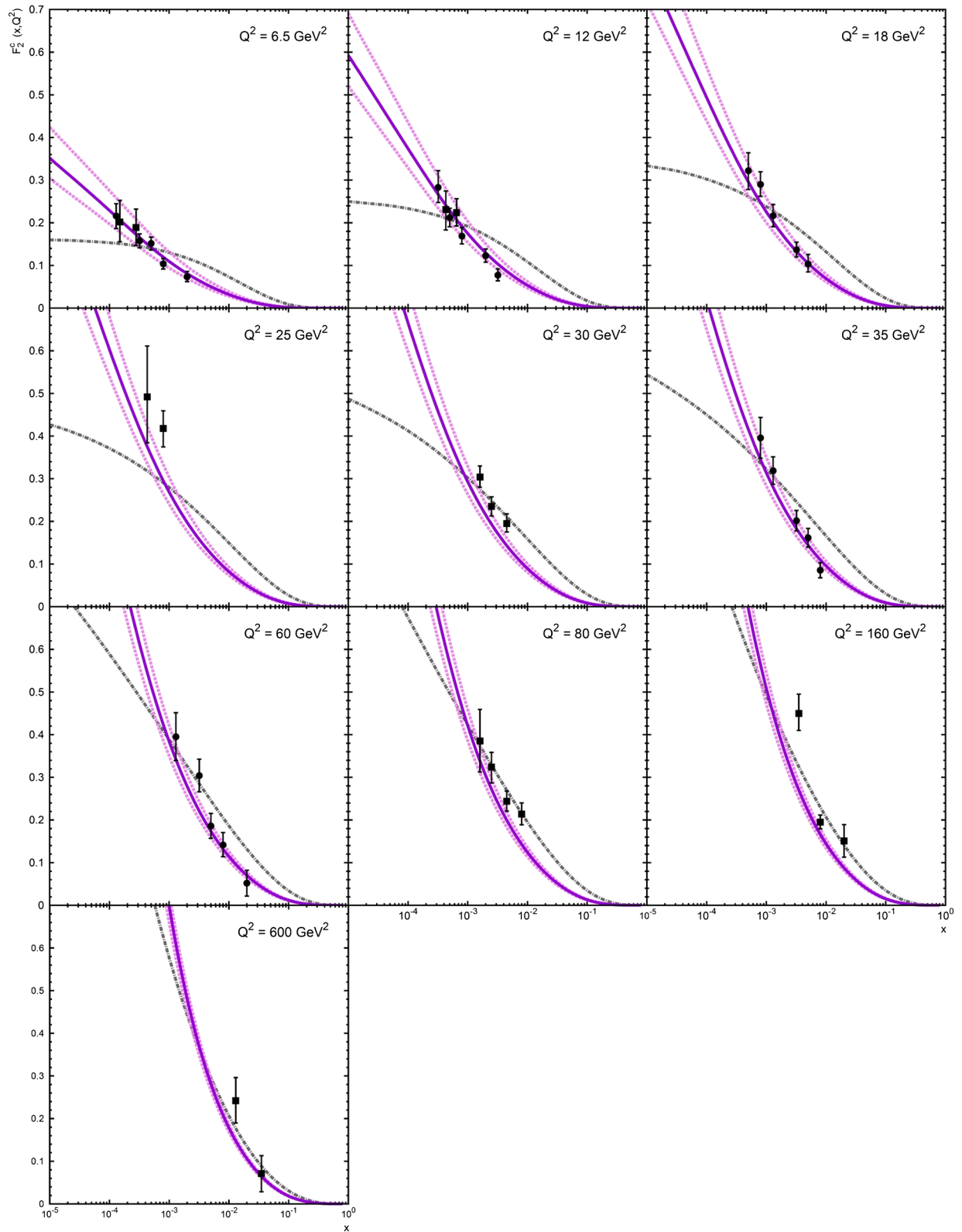
FIG. 5.   The charm contribution to the structure function $F_2(x, Q^2)$ as a function of x calculated at different Q^2. The notation of all curves is the same as in Fig. 4. The experimental data are from ZEUS [43] and H1 [44].
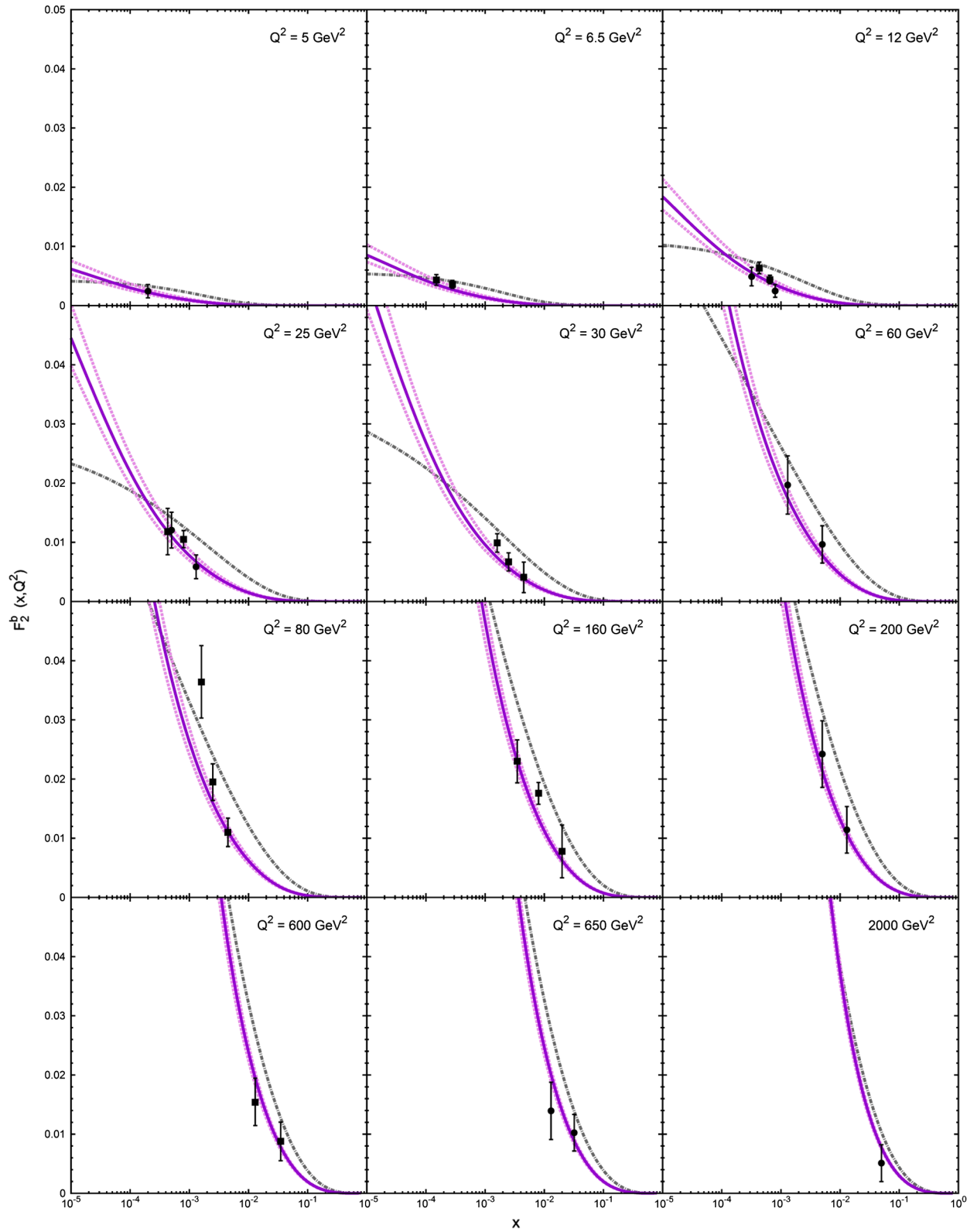
FIG. 6. The beauty contribution to the structure function $F_2(x, Q^2)$ as a function of x calculated at different Q^2. The notation of all curves is the same as in Fig. 4. The experimental data are from ZEUS [43] and H1 [45].

production at the LHC. The CMS Collaboration measured the b-jet cross sections in five b-jet rapidity regions, namely, $|y| < 0.5$, $0.5 < |y| < 1$, $1 < |y| < 1.5$, $1.5 < |y| < 2$, and $2 < |y| < 2.2$, as a function of the jet transverse momentum at $\sqrt{s} = 7\,\mathrm{TeV}$ [46]. The ATLAS Collaboration performed the measurements at central rapidities $|y| < 2.1$ [47].

Our main results are presented in Figs. 7 and 8, where we plot the calculated transverse momentum distributions of b jets compared to the LHC data as well as the corresponding data and theory ratios. We obtained a good description of the data using the MD2015 gluon distribution. The shape and absolute normalization of the measured b-jet cross sections are reproduced well. Moreover, the differential cross section
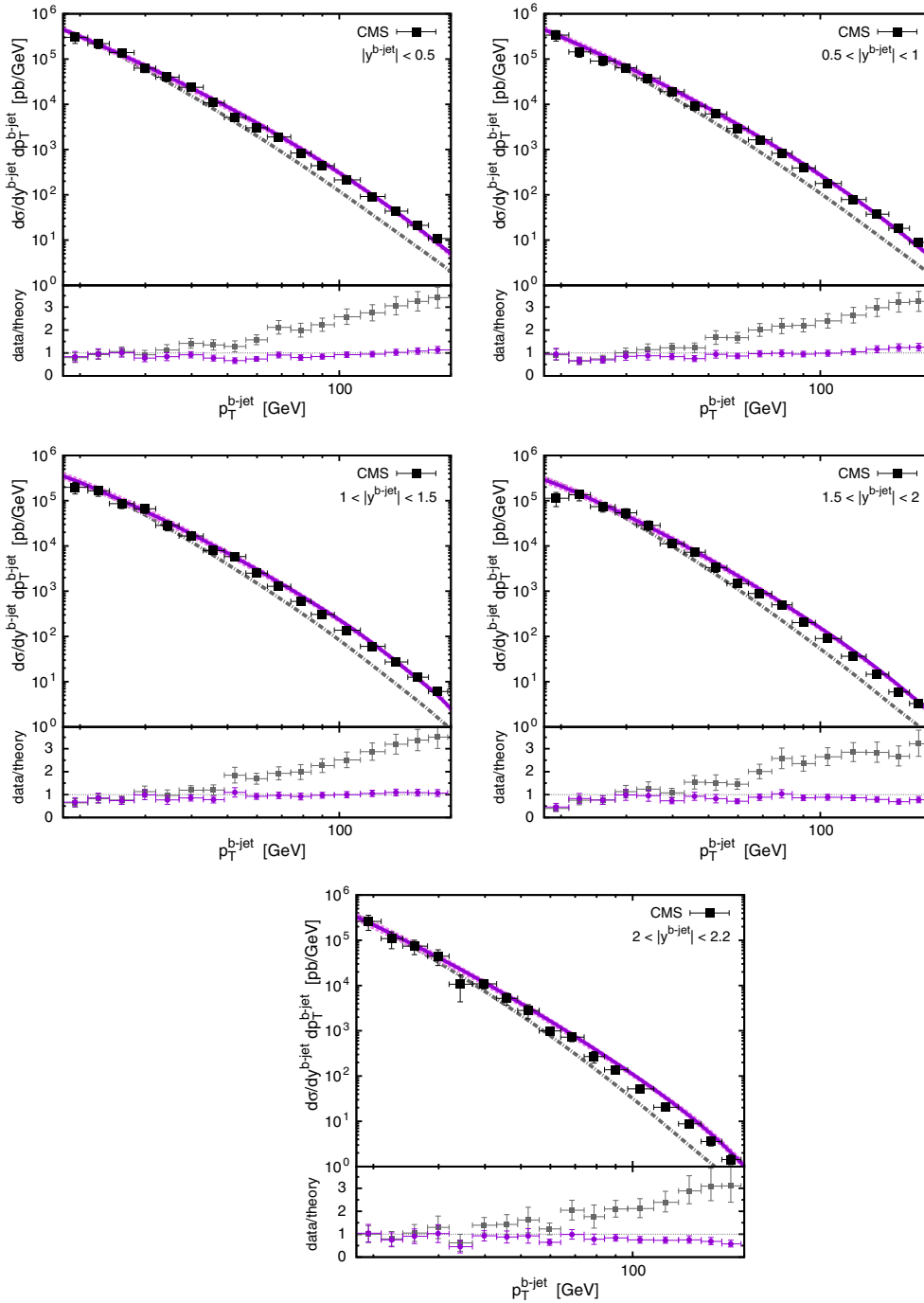

FIG. 7. The double differential cross sections $d\sigma/dy\,dp_T$ of the inclusive b-jet production as a function of the leading jet transverse momentum in different y regions. The used kinematical cuts are described in the text. The notation of all curves is the same as in Fig. 4. The experimental data are from CMS [46].
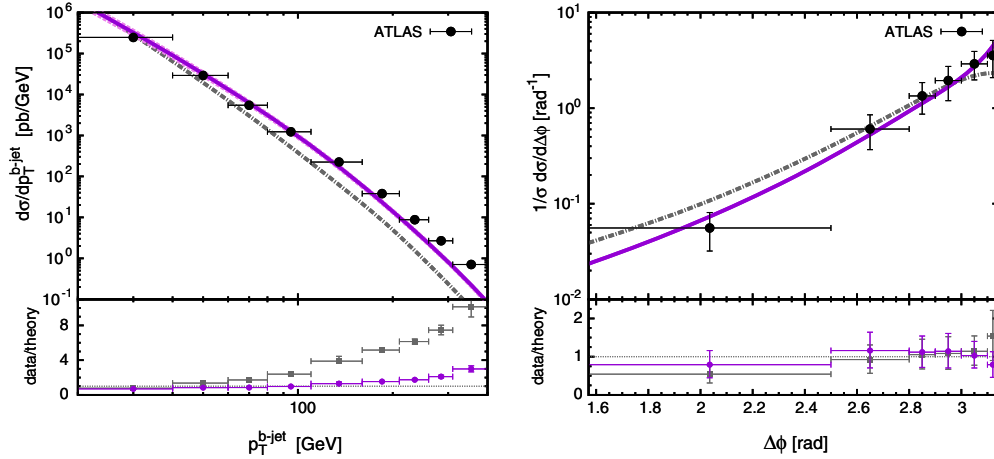
FIG. 8.   The distributions in the leading b-jet transverse momentum and azimuthal angle difference between the b jets produced at the LHC. The used kinematical cuts are described in the text. The notation of all curves is the same as in Fig. 4. The experimental data are from ATLAS [47].

as a function of the angular separation $\Delta\phi$ between two b jets measured at $p_T > 40$ GeV and $M > 110$ GeV, where M is the invariant mass of the produced $b\bar{b}$ pair, is also well described. This observable is known to be very sensitive to the $\mathbf{k}_T^2$ behavior of the TMD gluon distribution. The predictions based on the A0 gluon density lie below the data at high $p_T > 40$–50 GeV. Once again, we conclude that the best description of the LHC data [46,47] is achieved with the proposed MD2015 gluon density.

C. B^+ meson production

Besides the b-jet production, we probe the proposed MD2015 gluon density in the inclusive B^+ meson production at the LHC, which was measured by the CMS [48], ATLAS [49], and LHCb [50] Collaborations. Our basic formulas and the description of the calculation details are collected in Refs. [36,37]. Here we only note that we convert beauty quarks produced in the hard subprocess into B^+ mesons using the Peterson fragmentation function[2] with the usual shape parameter $\epsilon_b = 0.006$ [51]. Following Ref. [39], we set the branching fraction $f(b \to B^+) = 0.398$. The CMS Collaboration reported the total and differential B^+ cross sections measured at central rapidities $|y| < 2.4$ for $p_T > 5$ GeV and $\sqrt{s} = 7$ TeV [48]. The ATLAS Collaboration presented B^+ meson cross sections for $|y| < 2.25$ and $9 < p_T < 120$ GeV [49]. The LHCb Collaboration measured $B^\pm$ meson cross sections in the forward rapidity region $2 < y < 4.5$ at $p_T < 40$ GeV [50].

Our main results are presented in Figs. 9–11 compared with the LHC data and corresponding data and theory ratios. One can see that a good description of the B^+ meson transverse momentum and rapidity distributions is achieved using both TMD gluon densities under consideration. The results obtained with the MD2015 gluon density lie somewhat above the A0 ones and tend to slightly overestimate the measured cross sections at high transverse momenta but agree with the data within the uncertainties. However, both considered TMD gluon densities give similar behavior of the rapidity distributions. We would like to point out the remarkable description of the LHCb data in the forward rapidity region that extends essentially the applicability area of the proposed MD2015 gluon distribution.

D. D^* meson production

Similar to beauty quarks, charmed quarks are mainly produced at the LHC via the gluon-gluon fusion subprocess, and, therefore, the charm production cross section is also sensitive to the gluon density function. The transverse momentum distributions of several charmed mesons (D^*, $D^\pm$, D^0, D_s) were measured by the LHCb Collaboration at forward rapidities $2 < y < 4.5$ [52]. As a representative example, below we consider D^* meson production. To convert c quarks into D^* mesons, we apply the nonperturbative fragmentation function [53–55], which is often used in collinear QCD calculations. We set the branching fraction $f(c \to D^*) = 0.255$ [39].

Our numerical results are presented in Fig. 12. We find reasonably good agreement between our predictions obtained using the MD2015 gluon distribution and the LHCb data [52], which demonstrates again the wide area of its applicability. The A0 gluon density predicts flatter D^* transverse momentum distributions and does not contradict the data.

---

[2]Of course, the predicted transverse momentum distributions are sensitive to the quark-to-hadron fragmentation function. This dependence was studied earlier [36] and not considered in the present paper.
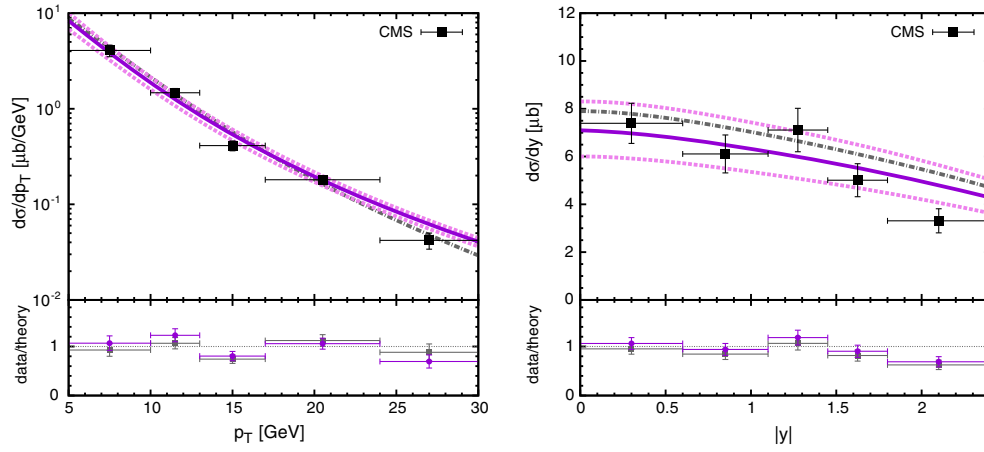
FIG. 9.   The transverse momentum and rapidity distributions of the B^+ meson production at the LHC. The used kinematical cuts are described in the text. The notation of all curves is the same as in Fig. 4. The experimental data are from CMS [48].
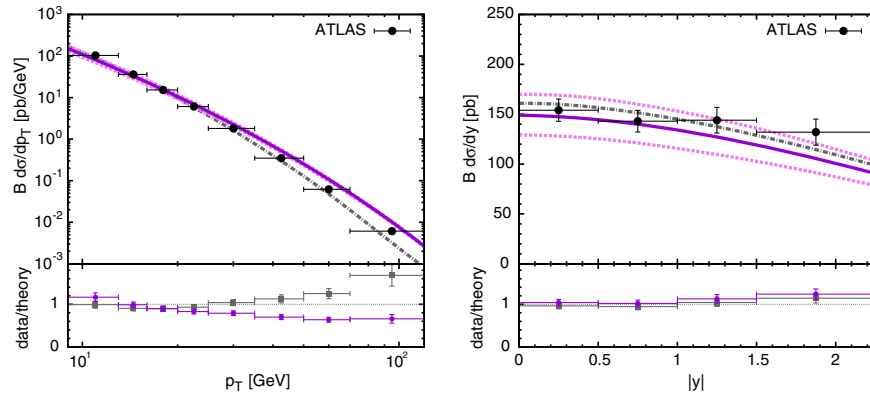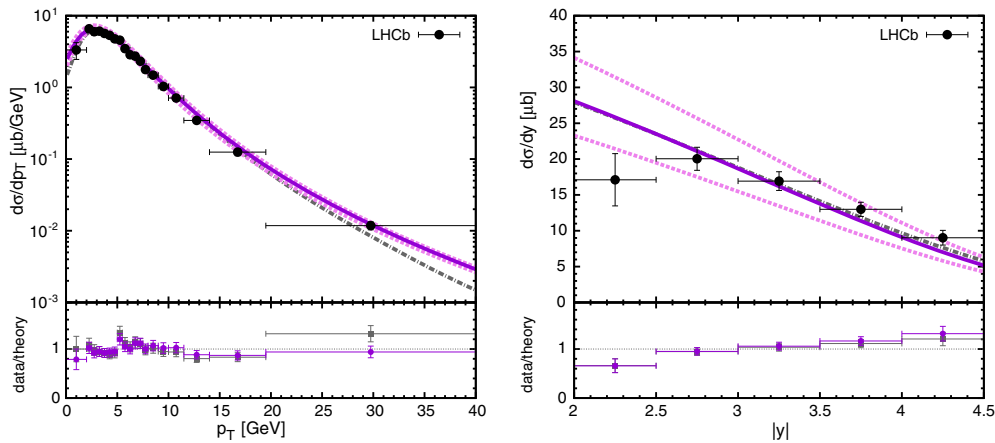

FIG. 10.   The transverse momentum and rapidity distributions of the B^+ meson production at the LHC. The used kinematical cuts are described in the text. The notation of all curves is the same as in Fig. 4. The experimental data are from ATLAS [49].

FIG. 11.   The transverse momentum and rapidity distributions of the $B^\pm$ meson production at the LHC. The used kinematical cuts are described in the text. The notation of all curves is the same as in Fig. 4. The experimental data are from LHCb [50].
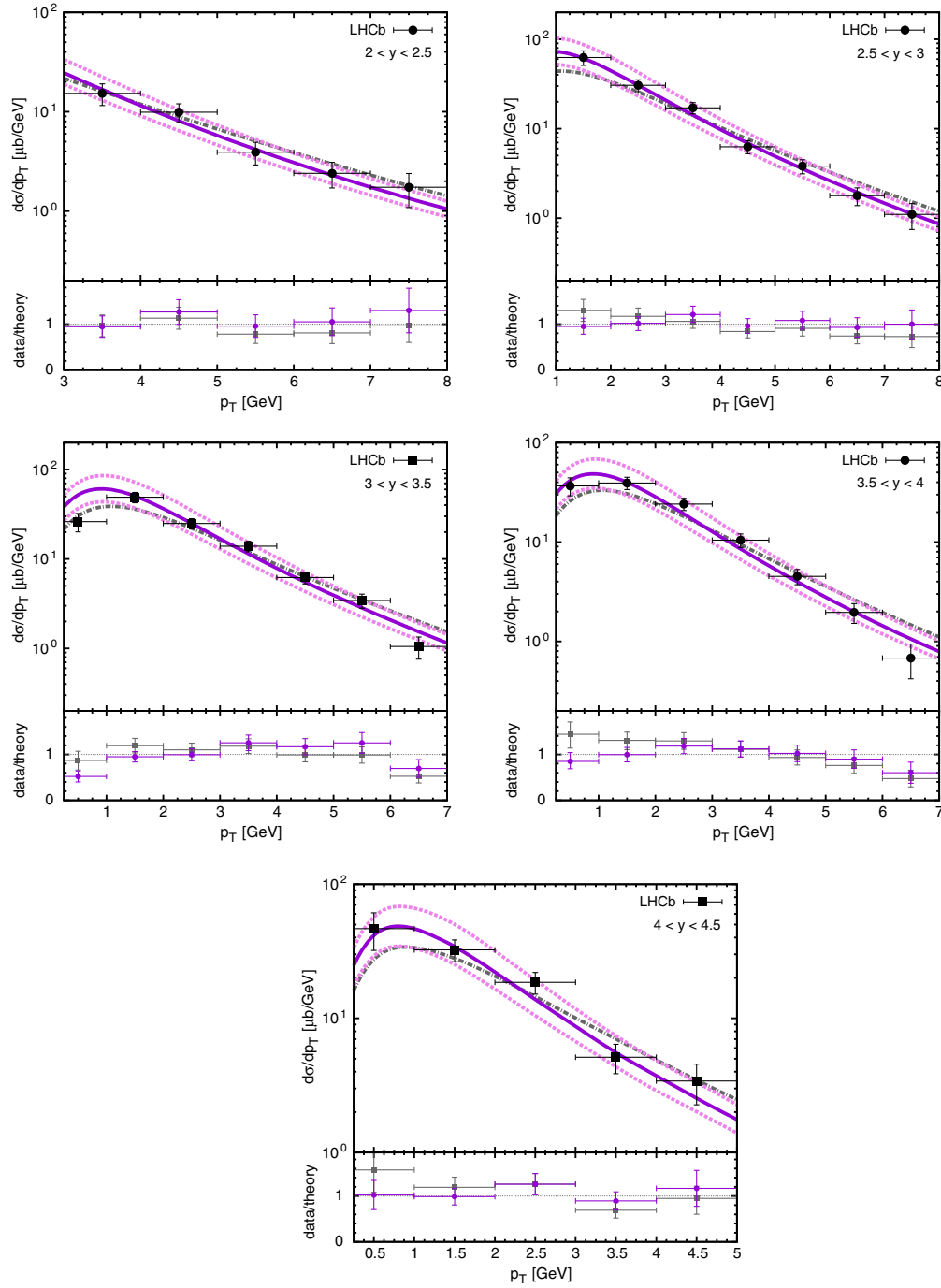
FIG. 12.   The transverse momentum distributions of the D^* meson production at the LHC. The used kinematical cuts are described in the text. The notation of all curves is the same as in Fig. 4. The experimental data are from LHCb [52].

E. Associated $W^{\pm}+$ jet and Z/γ^*+ jet production

Contrary to the processes considered above, where only the TMD gluon distribution was probed, the associated production of gauge ($W^{\pm}$ or Z) bosons and hadronic jets at the LHC offers high sensitivity to both quark and gluon density functions in the proton. The experimental data on the $W^{\pm}+$ jet and Z/γ^*+ jet production were obtained by the ATLAS Collaboration [56,57]. Below, we apply the TMD quark and gluon densities from the MD2015 set to describe

the LHC data. Our consideration is based on the off-shell amplitudes of the quark-gluon scattering subprocesses $qg^* \rightarrow W^{\pm}q'$ and $qg^* \rightarrow Z/\gamma^*q$ which include the subsequent decays $W^{\pm} \rightarrow l^{\pm}\nu$ and $Z/\gamma^* \rightarrow l^+l^-$ derived in Ref. [38]. Other details of the calculations can be found there.

The ATLAS data [56] on the associated $W^{\pm}$ and jet production refer to the kinematical region defined as $p_T^l > 25$ GeV, $|\eta^l| < 2.5$, $E_T^{miss} > 25$ GeV, $m_T(W) > 40$ GeV, $p_T^{jet} > 30$ GeV, and $|y^{jet}| < 4.4$, where $m_T(W)$
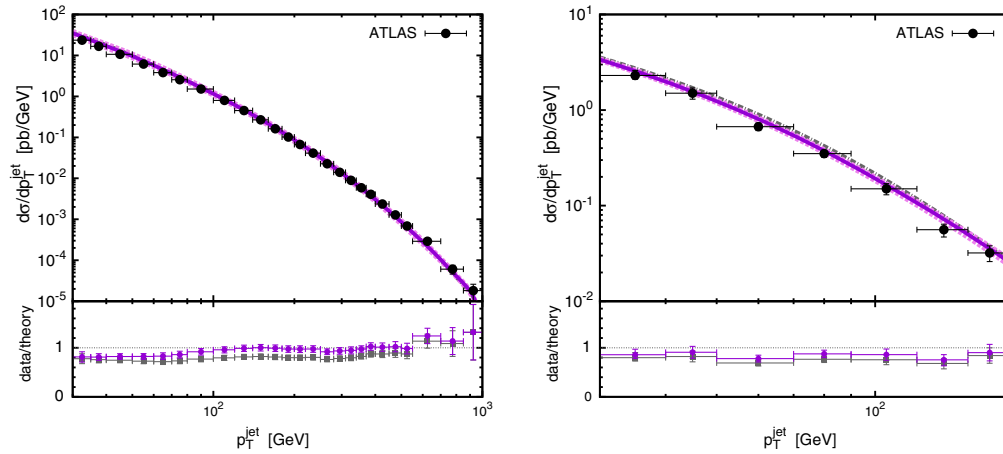
FIG. 13. The differential cross sections of associated the $W^{\pm}+$ jet (left panel) and $Z/\gamma^{*}+$ jet (right panel) production at the LHC as a function of the jet transverse momentum. The notation of all curves is the same as in Fig. 4. The used kinematical cuts are described in the text. The experimental data are from ATLAS [56,57].

is the transverse mass of the produced $W^{\pm}$ boson, η^{l} and p_{T}^{l} are the decay lepton pseudorapidity and transverse momentum, respectively, y^{jet} and p_{T}^{jet} are the rapidity and transverse momentum of the final hadronic jet, respectively, and E_{T}^{miss} is the missing transverse energy. The measurements of the $Z/\gamma^{*}+$ jet production were performed [57] at $66 < M < 116$ GeV, $p_{T}^{l} > 20$ GeV, $|\eta^{l}| < 2.5$, $p_{T}^{\text{jet}} > 20$ GeV, and $|y^{\text{jet}}| < 4.4$, where M is the invariant mass of the produced lepton pair. Our main numerical results are shown in Fig. 13 in comparison with the ATLAS data [56,57]. Additionally, we plot the corresponding data and theory ratios. We obtained a good description of these data with both TMD parton densities. The latter, in particular, demonstrates that the TMD quark and gluon distributions from the MD2015 set are reliable at relatively large scales, up to $\mu^{2} \sim m_{Z}^{2}$. However, we note that the full hadron-level Monte Carlo generator CASCADE [58], which uses the CCFM evolution equation for the initial state gluon emissions, is needed for a more detailed analysis of the associated production of gauge bosons and hadronic jets at the LHC. It is connected with a more accurate jet selection algorithm implemented in CASCADE, as was explained previously [38].

V. CONCLUSION

We fitted the experimental data on the inclusive spectra of the charged particles produced in the central pp collisions at the LHC to determine the TMD gluon density in a proton at the starting scale $\mu_{0}^{2} \sim 1$ GeV^{2}. We demonstrated that the best description of these spectra can be achieved by matching the derived TMD gluon distribution with the exact solution of the BFKL equation obtained at low x and small gluon transverse momenta outside the saturation region. Moreover, we established that the parameters of this fit did not depend on the initial energy in a wide energy interval. The average gluon transverse

momentum generated by this modified TMD gluon density is about 1.9 GeV in a wide region of x and is close to the nonperturbative QCD regime. Then, we extended the derived TMD gluon density to higher μ^{2} using a numerical solution of the CCFM gluon evolution equation. Additionally, we supplied the calculated TMD gluon density with the TMD valence and sea quark distributions. The latter was evaluated in the approximation where the gluon-to-quark splitting occurred at the last evolution step using the TMD gluon-to-quark splitting function. This function contains all single logarithmic small-x corrections in any order of the perturbation theory.

Special attention was paid to the phenomenological applications of the proposed MD2015 parton distributions to the hard processes. We considered the inclusive production of b jets, B^{+} and D^{*} mesons, and the associated production of $W^{\pm}$ or Z/γ^{*} bosons and hadronic jets at the LHC energies, and also the charm and beauty contribution to the proton structure function $F_{2}(x, Q^{2})$ and the longitudinal proton structure function $F_{L}(x, Q^{2})$. We demonstrated a significant influence of the initial nonperturbative gluon distribution on the description of the experimental data. We showed that the LHC data could be well described using the MD2015.

[1] L. V. Gribov, E. M. Levin, and M. G. Ryskin, Phys. Rep. **100,** 1 (1983); E. M. Levin, M. G. Ryskin, Yu. M. Shabelsky, and A. G. Shuvaev, Sov. J. Nucl. Phys. **53,** 657 (1991).

[2] S. Catani, M. Ciafaloni, and F. Hautmann, Nucl. Phys. **B366,** 135 (1991); J. C. Collins and R. K. Ellis, Nucl. Phys. **B360,** 3 (1991).

[3] B. Andersson *et al.* (Small-*x* Collaboration), Eur. Phys. J. C **25,** 77 (2002); J. Andersen *et al.* (Small-*x* Collaboration), Eur. Phys. J. C **35,** 67 (2004); J. Andersen *et al.* (Small-*x* Collaboration), Eur. Phys. J. C **48,** 53 (2006).

[4] J. C. Collins, *Foundations of Perturbative QCD* (Cambridge University Press, Cambridge, England, 2011).

[5] E. Avsar, Int. J. Mod. Phys. Conf. Ser. **04,** 74 (2011); arXiv:1203.1916.

[6] S. M. Aybat and T. C. Rogers, Phys. Rev. D **83,** 114042 (2011).

[7] F. Hautmann, M. Hentschinski, and H. Jung, Nucl. Phys. **B865,** 54 (2012).

[8] B. I. Ermolaev, M. Greco, and S. I. Troyan, Eur. Phys. J. C **71,** 1750 (2011); **72,** 1953 (2012).

[9] P. Kotko, K. Kutak, C. Marquet, E. Petreska, S. Sapeta, and A. van Hameren, J. High Energy Phys. 09 (2015) 106.

[10] A. A. Grinyuk, A. V. Lipatov, G. I. Lykasov, and N. P. Zotov, Phys. Rev. D **87,** 074017 (2013).

[11] A. V. Lipatov, G. I. Lykasov, and N. P. Zotov, Phys. Rev. D **89,** 014001 (2014).

[12] K. Golec-Biernat and M. Wüsthoff, Phys. Rev. D **59,** 014017 (1998); **60,** 114023 (1999).

[13] M. Ciafaloni, Nucl. Phys. **B296,** 49 (1988); S. Catani, F. Fiorani, and G. Marchesini, Phys. Lett. B **234,** 339 (1990); Nucl. Phys. **B336,** 18 (1990); G. Marchesini, Nucl. Phys. **B445,** 49 (1995).

[14] E. A. Kuraev, L. N. Lipatov, and V. S. Fadin, Sov. Phys. JETP **44,** 443 (1976); **45,** 199 (1977); I. I. Balitsky and L. N. Lipatov, Sov. J. Nucl. Phys. **28,** 822 (1978).

[15] V. N. Gribov and L. N. Lipatov, Sov. J. Nucl. Phys. **15,** 438 (1972); L. N. Lipatov, Sov. J. Nucl. Phys. **20,** 94 (1975); G. Altarelli and G. Parisi, Nucl. Phys. **B126,** 298 (1977); Yu. L. Dokshitzer, Sov. Phys. JETP **46,** 641 (1977).

[16] D. A. Artemenkov, G. I. Lykasov, and A. I. Malakhov, Int. J. Mod. Phys. A **30,** 1550127 (2015); arXiv:1504.07841.

[17] V. A. Bednyakov, A. A. Grinyuk, G. I. Lykasov, and M. Poghosyan, Int. J. Mod. Phys. A **27,** 1250042 (2012).

[18] Yu. V. Kovchegov, Phys. Rev. D **61,** 074018 (2000).

[19] A. B. Kaidalov, Z. Phys. C **12,** 63 (1982); Surv. High Energy Phys. **13,** 265 (1999); A. B. Kaidalov and O. I. Piskunova, Z. Phys. C **30,** 145 (1986); Yad. Fiz. **43,** 1545 (1986).

[20] G. I. Lykasov and M. N. Sergeenko, Z. Phys. C **56,** 697 (1992); **52,** 635 (1991); **70,** 455 (1996).

[21] V. A. Bednyakov, G. I. Lykasov, and V. V. Lyubushkin, Europhys. Lett. **92,** 31001 (2010); arXiv:1005.0559.

[22] NA61 Collaboration, Eur. Phys. J. C **74,** 2794 (2014).

[23] ATLAS Collaboration, New J. Phys. **13,** 053033 (2011); CMS Collaboration, Phys. Rev. Lett. **105,** 022002 (2010).

[24] V. S. Fadin and L. N. Lipatov, Phys. Lett. B **429,** 127 (1998).

[25] M. Ciafaloni and G. Camici, Phys. Lett. B **430,** 349 (1998).

[26] D. N. Triantafyllopoulos, Nucl. Phys. **B648,** 293 (2003).

[27] M. Deak, F. Hautmann, H. Jung, and K. Kutak, arXiv:1012.6037.

[28] M. Deak, F. Hautmann, H. Jung, and K. Kutak, Eur. Phys. J. C **72,** 1982 (2012).

[29] A. D. Martin, W. J. Stirling, R. S. Thorne, and G. Watt, Eur. Phys. J. C **63,** 189 (2009).

[30] F. Hautmann, H. Jung, and S. Taheri Monfared, Eur. Phys. J. C **74,** 3082 (2014).

[31] S. Catani and F. Hautmann, Nucl. Phys. **B427,** 475 (1994); Phys. Lett. B **315,** 157 (1993).

[32] G. Curci, W. Furmanski, and R. Petronzio, Nucl. Phys. **B175,** 27 (1980).

[33] F. Hautmann, M. Hentschinski, and H. Jung, arXiv:1207.6420.

[34] H. Jung, arXiv:hep-ph/0411287.

[35] A. V. Kotikov, A. V. Lipatov, G. Parente, and N. P. Zotov, Eur. Phys. J. C **26,** 51 (2002); A. V. Kotikov, A. V. Lipatov, and N. P. Zotov, Eur. Phys. J. C **27,** 219 (2003).

[36] H. Jung, M. Kraemer, A. V. Lipatov, and N. P. Zotov, Phys. Rev. D **85,** 034035 (2012).

[37] N. P. Zotov, A. V. Lipatov, and V. A. Saleev, Phys. At. Nucl. **66,** 755 (2003); S. P. Baranov, N. P. Zotov, and A. V. Lipatov, Phys. At. Nucl. **67,** 837 (2004).

[38] A. V. Lipatov and N. P. Zotov, Phys. Rev. D **90,** 094005 (2014); A. V. Lipatov, M. A. Malyshev, and N. P. Zotov, J. High Energy Phys. 12 (2011) 117.

[39] PDG Collaboration, Chin. Phys. C **38,** 090001 (2014).

[40] G. P. Lepage, J. Comput. Phys. **27,** 192 (1978).

[41] H1 Collaboration, Eur. Phys. J. C **74,** 2814 (2014).

[42] ZEUS Collaboration, Phys. Lett. B **682,** 8 (2009).

[43] ZEUS Collaboration, J. High Energy Phys. 09 (2014) 127.

[44] H1 Collaboration, Eur. Phys. J. C **71,** 1769 (2011); **72,** 2252 (2012).

[45] H1 Collaboration, Eur. Phys. J. C **65,** 89 (2010).

[46] CMS Collaboration, J. High Energy Phys. 04 (2012) 084.

[47] ATLAS Collaboration, Eur. Phys. J. C **71,** 1846 (2011).

[48] CMS Collaboration, Phys. Rev. Lett. **106,** 112001 (2011); J. High Energy Phys. 03 (2011) 090.

[49] ATLAS Collaboration, J. High Energy Phys. 10 (2013) 042.

[50] LHCb Collaboration, J. High Energy Phys. 08 (2013) 117.

[51] C. Peterson, D. Schlatter, I. Schmitt, and P. Zerwas, Phys. Rev. D **27,** 105 (1983).

[52] LHCb Collaboration, Nucl. Phys. **B871,** 1 (2013).

[53] M. Cacciari and P. Nason, Phys. Rev. Lett. **89,** 122003 (2002); M. Cacciari, S. Frixione, M. L. Mangano, P. Nason, and G. Ridolfi, J. High Energy Phys. 07 (2004) 033.

[54] M. Cacciari and P. Nason, J. High Energy Phys. 09 (2003) 006.

[55] E. Braaten, K.-M. Cheng, S. Fleming, and T. C. Yuan, Phys. Rev. D **51,** 4819 (1995).

[56] ATLAS Collaboration, Eur. Phys. J. C **75,** 82 (2015).

[57] ATLAS Collaboration, Phys. Rev. D **85,** 032009 (2012).

[58] H. Jung, Comput. Phys. Commun. **143,** 100 (2002); H. Jung *et al.*, Eur. Phys. J. C **70,** 1237 (2010).